Article

Cold Rolling Technology Optimization for EN AW 4343/3003/4343 Cladded Aluminum Alloys and Influence of Parameters on Microstructure, Mechanical Properties and Sustainable Recyclability

Bojan Kropf [1,2,3], Peter Cvahte [1,4], Matija Arzenšek [1,3] and Jakob Kraner [1,3,4,*]

1 Impol Aluminium Industry, Partizanska 38, SI-2310 Slovenska Bistrica, Slovenia
2 Faculty of Mechanical Engineering, University of Maribor, Smetanova 17, SI-2000 Maribor, Slovenia
3 Department of Materials and Metallurgy, Faculty of Natural Sciences and Engineering, University of Ljubljana, Aškerčeva cesta 12, SI-1000 Ljubljana, Slovenia
4 Institute of Metals and Technology, Lepi pot 11, SI-1000 Ljubljana, Slovenia
* Correspondence: jakob.kraner@impol.si

Abstract: The present study investigates the accumulative roll bonding process applied to the EN AW 3003 aluminum alloy, serving as a composite material on both sides and consisting of the EN AW 4343 aluminum alloy. For the characterization of the optical microscopy, corrosion tests with saltwater acetic acid and mechanical properties before and after the braze test were employed. The numerical simulations accurately predicted the industrial cold rolling values for the rolling force and surface temperature. The most comprehensive understanding of the cold rolling parameters for both side-cladded materials was achieved by combining predictions for cladded and uncladded materials. The thickness of the cladded layer presented as a percentage after roll bonding was 18.7%. During the cold rolling and annealing, the cladded thickness was increased to 24.7% of the final 0.3 mm of the total cold-rolled product thickness. According to the performed braze test for final thickness, the ultimate tensile strength and yield strength were decreased, and the elongation increased to 18.1%. In addition to the described changes in mechanical properties, the material's anisotropy improved from 5.4% in the cold-rolled condition to 2.0% after the braze test. After multiple re-meltings of the cladded material, the analyzed chemical compositions allow for recycling and reuse as different 4xxx, 5xxx, and 6xxx alloys.

Keywords: aluminum alloys; numerical simulations; cladding; characterization; recycling

1. Introduction

The emphasized importance of e-mobility currently leads to larger electric vehicle (EV) production [1]. EVs have, in comparison to fossil fuel vehicles, a larger number of heat-exchanging components (cooling plate, chiller), which are most often made from aluminum-cladded materials for brazing applications [2]. Everything from the production of cladded material to the final brazed product and its installation in the EV present challenges on an interdisciplinary technical scale [3–5].

The aluminum-cladded sheet for braze application in the automotive industry is typically a (sandwich) structure with two or more layers, where the clad sheets are bonded to the core alloy on one or more surfaces [6]. The most common alloy combinations for cladding are EN AW 3003 with EN AW 4343 [7] or any other modified 3xxx or 4xxx aluminum alloy. In comparison to the mentioned reference, numerical simulated and industrial cold rolling has been optimized as a novelty in the studies published so far. Kang et al. [8] successfully extended the cladding of materials by incorporating EN AW 6111 between EN AW 3003 and EN AW 4343. The age-hardened alloy enhances mechanical properties during brazing, performed at a temperature close to the melting point for a short

duration (600 °C—3 min) [9]. Further, the reuse of brazed aluminum-rolled products was not often considered. For the first time, concrete cases for sustainable recycling of cladded aluminum alloys are presented in this paper. The interesting combination of the two-side cladded 5xxx aluminum alloy with the commercial 6xxx aluminum alloy was created by Kim et al. [10]. EN AW 7075 was used for a cladded structure by Zhang et al. [11]. The results of their investigation show that the role of EN AW 7075 in the clad structure is to increase the maximum flow stress of the core alloy with the increased temperature during hot rolling for bonding.

The bonding of different aluminum alloys for braze-used products can be performed via the already mentioned hot rolling [12], where the bond criterion and its correlated parameters can be predicted. Movahedi et al. [13] studied the roll bonding behavior of EN AW 3003 with EN AW 4043 and EN AW 3003 with a Zn sheet and concluded that the first-mentioned clad combination was bonded with higher joint strengths and lower threshold reductions in thickness compared to the second mentioned analyzed cladded combination. The evolution of the grain structure in both-sided clad EN AW 3003 with EN AW 4343 was investigated by Kim et al. [14], but the comparison of corrosion resistance for cold-rolled and post-brazed material was not reported, and that is the novelty in this article. They compared the grain structures of low-reduction and high-reduction cold-rolled clad materials and concluded that higher reduction results in fewer coarse elongated grains in the microstructure compared to low reduction. Cha et al. [15] studied the interfacial effects of heat treatments on the mechanical properties of the clad material. The EN AW 7075 cladded from both sides with EN AW 6022 has significantly improved strength and elongation after heat treatment because of the activated precipitations and diffusion of major alloying elements in comparison to the as-rolled (bonded) sheet.

The literature review highlights a notable gap in the recycling possibilities for clad aluminum alloys. This issue becomes increasingly significant with the growth of electric vehicles (EVs) and the growing emphasis on sustainability. Notably, Raabe et al. [16] delve into the science of so-called 'dirty' alloys, addressing the challenges associated with them. Additionally, Pilipenets et al. [17] provide insights into various opportunities for upcycling aluminum composite panels. This paper contributes by presenting new potential reuses for aluminum-clad material, both as pre-consumer and post-consumer scrap.

The primary focus of this article is the production and characterization of aluminum-clad material. The EN AW 3003 aluminum alloy was, during hot rolling, cladded with EN AW 4343 aluminum alloy from both sides. The 6 mm hot-rolled band was further cold rolled after the numerical simulation's prediction and after the comparison with the temperatures and rolling forces of industrial cold rolling. The novelty of this research is the successful cold rolling technology planning according to the numerical simulations, supported directly with the multi-layer materials' properties. The clad material at a final thickness of 0.3 mm was metallographically analyzed and tested for the corrosion and mechanical properties as cold rolled and after brazing, simulating stage material. The final part of the research attended to the recycling possibilities of aluminum-cladded material. With laboratory re-melting and chemical analysis, the possibilities for creating different aluminum alloys were revealed, and they can be discussed as an important research contribution.

2. Materials and Methods

2.1. Design of the Rolling Process

The cladding process was performed on the hot rolling mill of the Impol-TLM company (Šibenik, Croatia). A structure for the aluminum-clad sheet was created, consisting of a 490 mm thick slab of EN AW 3003 and two plates of EN AW 4343, each with a thickness of 50 mm, as illustrated in Figure 1. The chemical compositions of both used aluminum alloys were determined with the optical emission spectrometer ARL 4460 (Thermo Fisher Scientific, Waltham, MA, USA) and are presented in Table 1. The whole structure was homogenized with the regime at a temperature of 540 °C for 6 h. The successful cladded structure with hot rolling (total of 19 passes from initial 500 °C to 380 °C temperature

after the last pass) was finished on the 6 mm hot-rolled band (Figure 1). In the last step, cylindrical samples with a diameter of 5 mm and a height of 6 mm were obtained from the hot-rolled band. These samples were utilized in compression tests conducted on a dilatometer Bähr DL 805A/D (TA Instruments, New Castle, DE, USA) to generate stress–strain curves. These curves were essential for calculating the factors (*m1*, *m2*, *m3*, and *m4*) in the Hansel–Spittel equation, serving as descriptors of the material's mechanical properties for numerical simulations. According to the obtained stress–strain curves from dilatometry, the factors in the Hansel–Spittel Equation (1), which are sufficient for material inventory during cold forming, where T is temperature, ε is strain, and $\dot{\varepsilon}$ is strain rate [18], for the material property description in numerical simulations, were calculated for cladded EN AW 3003 aluminum alloy and compared with the uncladded EN AW 3003 aluminum alloy for the cold rolling technology scheduling.

$$\sigma_F = A \cdot e^{m1T} \cdot \varepsilon^{m2} \cdot \dot{\varepsilon}^{m3} \cdot e^{\frac{m4}{\varepsilon}} \tag{1}$$

A custom-made model for numerical simulations was used, where the rolling machine specifics (work roll diameter, friction coefficient, speed) and material properties and behavior were taken into account. The cold rolling (total of 6 passes) was performed at Impol-FT company (Slovenska Bistrica, Slovenia) down to 0.3 mm (Figure 1) with one intermediate annealing (380 °C—1 h), according to the numerical simulation technology. Samples for mechanical properties and metallographic characterization were taken during cold rolling, with total deformation gradually increasing over the course of the process. The temperature after cold rolling was measured directly on the coil with the Testo 735-2 thermometer (Testo, Titisee-Neustadt, Germany) with the K-type thermocouple sensor. The post-brazing simulation was conducted using the final thickness of the material, wherein the material was subjected to a temperature of 600 °C for 3 min in a laboratory furnace (laboratory braze test). The material with so-called post-braze properties is similar or must be reached when the cladded sheet is brazed and used for HVAC (or any other application). The final laboratory heat treatment (600 °C for 3 min) does not have any connection with the successful hot roll bonding, but it is the method for quality control of cladded material in the case of semi-products.
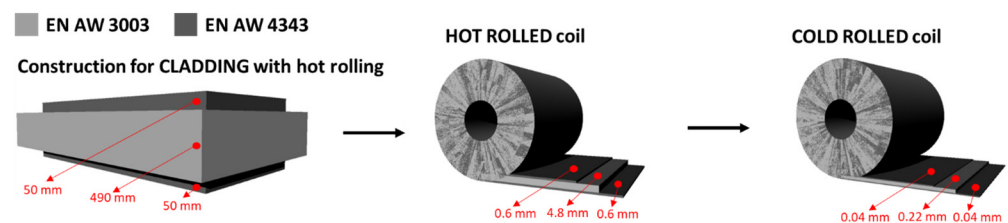

Figure 1. Schematic presentation of production process.

Table 1. Chemical composition of 3003 and 4343 used Al alloys (wt.%).

Alloy	Mn	Si	Fe	Mg	Cu	Ti	Al
3003-CORE	1.19	0.18	0.46	0.02	0.08	0.02	Bal.
4343-CLAD	0.03	6.94	0.39	0.02	0.02	0.02	Bal.

2.2. Characterization

The microstructure was observed in the cross-section so that the thicknesses of core and clad materials were analyzed. The metallographic preparation followed mechanical grinding, polishing, and electrochemical etching with Barker's solution. The metallographically prepared samples were observed with the light microscope (LM) under polarized reflection of Zeiss Axio Observer (Carl Zeiss AG, Jena, Germany). The thickness of the cladded layer was measured at ten different positions among the whole sample. In accordance with ASTM E8M, the cladded material was tensile-tested in the rolling direction. The specimens

had a typical bone shape appropriate for testing method B and determination of ultimate tensile strength (UTS), yield strength (YS), and elongation (A). For each cladded material thickness, five specimens were tested. For the anisotropy test (Erichsen cupping test), five repetitions for each tested material were also performed, and the results are presented as averages. The anisotropy indicator (*Ear*) was determined automatically according to ISO 20482:2013 for metallic materials sheet and strip Erichsen cupping test. First, the cups were extracted with the Erichsen 134 (Erichsen GmbH & Co, Hemer, Germany). The cups were then put in the special measurement equipment Erichsen 126 plus (Erichsen GmbH & Co, Hemer, Germany), where the radius and height of ears on the cup were measured. From these data, the *Ear* value is obtained and presented as the anisotropy of the analyzed material in %. The corrosion tests of the cladded aluminum samples were performed with the electrochemical potentiodynamic technique. The observed cold-rolled and simulated brazed samples had an exposed area of 1 cm^2. Electrochemical measurements were conducted using a 5% NaCl solution, which is standard for the Saltwater Acetic Acid Test (SWAAT). A three-electrode system was used, where the aluminum sample was the working electrode, a Pt mesh presented the counter electrode, and a saturated calomel electrode (SCE) was used as the reference electrode. Before the corrosion measurements, the surface of the samples was prepared in the same way as for the metallographic analysis (grinding, polishing). All the potentiodynamic polarization data with a scan rate of 1 mV/s were processed with software to compare the electrochemical parameters of corrosion current density (*icorr*), corrosion potential (*Ecorr*), and corrosion rate (*vcorr*). For each compared material, we performed five repetitions of quick corrosion tests. The recycling possibility of cladded material was researched with the material remelting in the laboratory melting furnace with the cooling curve analysis and determination of chemical composition with the optical emission spectrometer after each of three remeltings.

3. Results and Discussion

3.1. Compression Tests

The compression tests were performed at room temperature (25 °C) (solid curves) and elevated temperature (200 °C) (dashed curves). Three different strain rates (0.1 s^{-1} (red), 1 s^{-1} (green), and 10 s^{-1} (blue)) were used. The results are presented as stress–strain diagrams in Figure 2. It can be observed that at 25 °C, higher stress was reached at the same strain as at the elevated temperature of 200 °C, as expected. For the 200 °C tests, the highest value was 151 MPa, whereas for the 25 °C tests, the highest achieved stress value was 211 MPa. Furthermore, there is a trend which is seen as an increase in stress with strain. The same analogy follows the rate-dependent relation of stress–strain curves at different strain rates. Higher strain rates (from 0.1 s^{-1} to 10 s^{-1}) lead to an increase in the material's elasto-viscoplastic response, that is, stress.

From the results of compression tests, as presented in Figure 2, the factors of the Hansel–Spittel equation (Table 2) were calculated and used as a description of the material's mechanical properties for numerical simulation. In the comparison of the mentioned factors for cladded and uncladded EN AW 3003, it is shown that factor *A* is higher for the cladded material, as expected. The highest difference is observed in factors *m2* and *m4*, which are connected to the strain hardening component of the Hansel–Spittel equation. The *m1* factor of uncladded and cladded material shows a similar value in both cases. Factor *m1* is connected to temperature softening, which would correspond to a greater softening effect in cladded material, due to a slightly more negative value in the case of cladded 3003. The *m3* factor is connected to a strain rate-dependent stress response, meaning that uncladded 3003 exhibits a greater strain rate dependency than the cladded 3003 material.

Table 2. Hansel–Spittel equation factors for cladded and uncladded EN AW 3003.

	A	*m1*	*m2*	*m3*	*m4*
Uncladded 3003	213.092	−0.00196	0.11707	0.02415	−0.01439
Cladded 3003	233.234	−0.00237	0.16832	0.01938	−0.00213
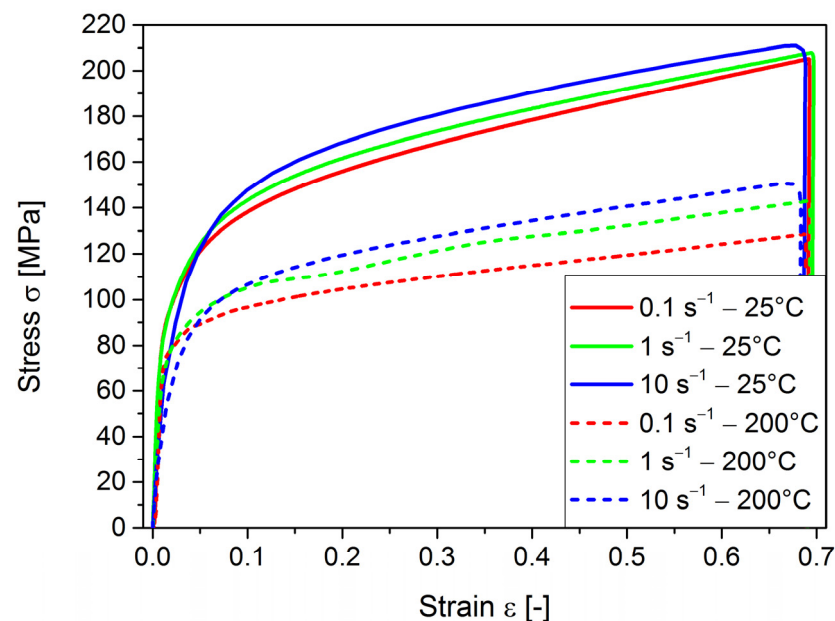
Figure 2. Stress–strain (σ−) curves from compression test for hot bonded material at different temperatures (25 °C and 200 °C) and strain rates (0.1 s^{-1}, 1 s^{-1} and 10 s^{-1}).

3.2. Numerical Simulation

The results of the numerical simulations, compared to the industrially measured values for rolling force during cold rolling, are presented in Figure 3a. The gradual reduction in the rolling force is accordingly present for both simulated and industrially measured values. The highest predicted rolling force (5200 kN) appears for the first pass of the uncladded alloy. For the same alloy cladded on both sides, the predicted rolling forces are lower and in the range of 4800 kN for the first pass to 1800 kN for the sixth pass. Observing the industrially measured rolling forces, they are much more correlated with the cladded 3003 values, with the exception of the second pass, where the rolling force as measured industrially is exactly the same as for the uncladded 3003 material. The values of surface temperature (Figure 3b) of the industrially measured temperatures match more with the predicted temperatures for the uncladded alloy. The temperatures after the first pass are, in all three cases, the lowest. The industrially measured temperatures and the predicted temperatures for uncladded material do not differ by more than 10 °C and reach the highest temperature after the fourth pass (140 °C). The predicted temperatures for the cladded 3003 alloy were, especially after the second, third, and fourth pass, significantly higher than the industrially measured temperatures. The highest predicted surface temperature for cladded alloy is 190 °C.

Reviews of recent advances and trends in aluminum-cladded numerical models predominantly discuss the bonding behavior and quality of rolled structures [19]. There is more attention during research on texture evolution [20] and experimental verification of accumulative roll bonding [21] than for already cladded and further cold-rolled products. From the results of our numerical simulations, which were compared with the industrial measurements of rolling force and surface temperature, the most rational explanation of rolling parameters for EN AW 3003 cladded on both sides with EN AW 4343 was made as a combination of cladded and uncladded material predictions. The rolling force from industrial measurements fits more with the numerical simulated predictions of cladded

3003 material, despite the measured surface temperature being more correlated with the uncladded 3003 material used in the numerical simulation.
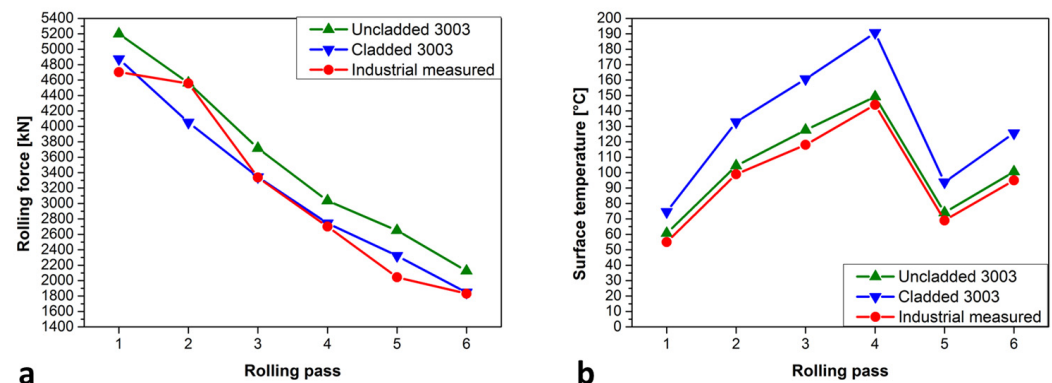

Figure 3. Comparison of numerical simulations results for cladded and uncladded EN AW 3003 aluminum alloy and industrial measurements for EN AW 3003 cladded on both sides with EN AW 4343: (**a**) rolling force; (**b**) surface temperature.

3.3. Microstructural Characteristics

Figure 4 illustrates the proportion of the cladded layer on both sides relative to the thickness of the rolled material. The deviation of the measured cladded thickness, presented as a share of the overall thickness of the rolled product, is also depicted. Dashed lines mark the permissible thicknesses or shares for cladded layers. It is observed that the basic percentage of the cladded layer increases with a decrease in material thickness, as noted by Kim et al. [22]. Following hot rolling, the material with cladding on both sides exhibits an 18.7% cladded share. Upon reduction to 3.5 mm, the cladded share minimally increases to 19%. Subsequent additional cold deformation raises the cladded share to 22%, and with further reduction, it decreases to 19.9%. Before intermediate annealing at a thickness of 0.8 mm, the cladded share again rises to 22.2%, but after annealing at the same thickness, it decreases to 20.5%. This can be attributed to the blurred border between the core and cladded material, given the activation of grain growth, especially in the cladded material of the core layer [23]. Following annealing and subsequent cold rolling to the final thickness, the cladded share increases to over 24%.
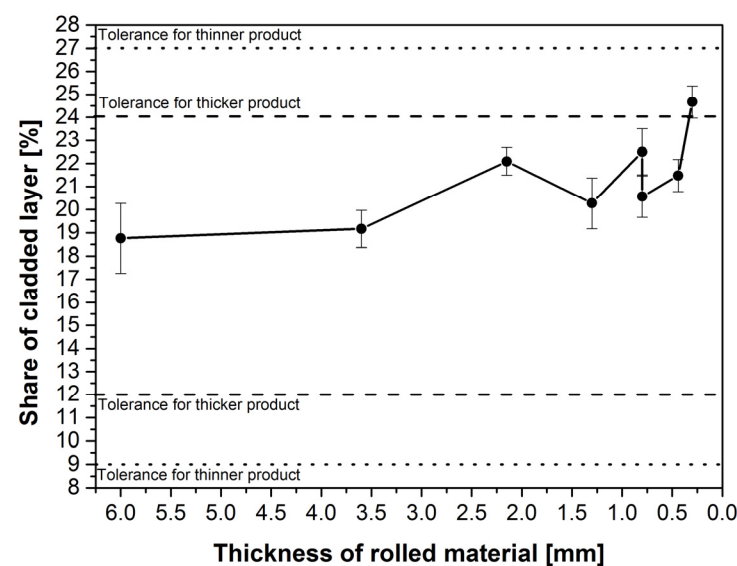

Figure 4. Presentation of cladded layer (%) in dependence of total material thickness (mm).

Observing Figure 5a, the microstructure of the cold-rolled condition is presented. The border between the core and cladded material is clearly visible. The grains in the microstructure are deformed with a longitudinal shape in the rolling direction in all three layers. In Figure 5b, the microstructure of the cladded material after the braze test is presented. The grains in the core and cladded layers are recrystallized and round. The grains in the cladded layers are significantly bigger than in the core, giving the impression that the grains in the cladded layers were melted and retook the shape of dendrites. The border between the core and cladded layers is less significant after the braze test compared to the cold-rolled condition, since the grains (dendrites) according to the Ostwald ripening [24] interfered with the core layer.
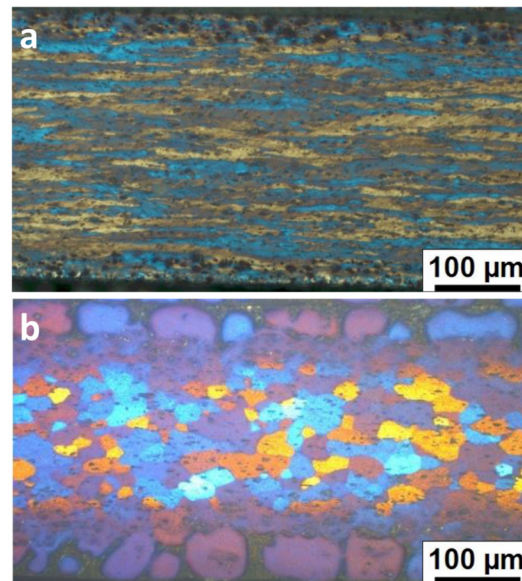
Figure 5. Microstructure of both aluminum alloy EN AW-3003 cladded on both sides with the EN AW-4343, with the total thickness 0.3 mm: (**a**) after cold rolling; (**b**) after braze test.

3.4. Mechanical Properties and Anisotropy

The mechanical and anisotropic properties of the cold-rolled and post-braze testing (600 °C—3 min) cladded material at the final thickness of 0.3 mm are presented in Table 3. The ultimate tensile strength (UTS) value for the cold-rolled state is 215 MPa. After the braze test, the UTS is decreased to 146 MPa. The described decrease in UTS is, according to the grain size growth after the braze test, not unexpected. Similar to the UTS trend, the yield strength (YS) value is decreased from 199 MPa to 57 MPa after the braze test. In accordance with the UTS and YS reduction, the elongation (A) is increased. Initially, the A is 2.4%, and it increases to 18.1% after the braze test. In contrast, the anisotropy indicator value (*Ear*) is decreased after the braze test. In the cold-rolled state, the material has 5.4% of *Ear*, and after the braze test, it reaches only 2.0% of *Ear*, which is indicative of quite isotropic material after heat treatment. Despite the short heat treatment at high temperature strongly decreasing the UTS and YS, a positive effect on the reduction in anisotropy is observed, which can be connected to the complex, more layered material texture.

Table 3. Results of mechanical and formability tests for cold-rolled and post-braze testing analyzed cladded material.

	Mechanical Properties			Anisotropy
	UTS [MPa]	YS [MPa]	A [%]	E_{ar} [%]
Cold-rolled	215	199	2.4	5.4
Braze-tested	146	57	18.1	2.0

3.5. Corrosion Behavior

The corrosion behavior, measured as the corrosion potential E_{corr}, in terms of the dependence of current density i_{corr} curves of the compared cold-rolled and post-braze testing (600 °C—3 min) states is presented in Figure 6. More detailed results are listed in Table 4. The difference between E_{corr} of cold-rolled and post-brazing test materials is −10 mV. The difference between the mentioned samples is higher for the potential for pitting corrosion, represented by the E_{pit} value. E_{pit} is less negative for the sample after the braze test. For the re-passivation, potential E_{rep} values differ the least in comparison with the previously stated E_{corr} and E_{pit} values. The consequence of the quite similar values of E_{corr} and E_{rep} for cold-rolled and post-brazing test materials is that the calculated difference is imperceptible. In contrast to the different corrosion potentials, the i_{corr} values for the compared material states are quite different. For the cold-rolled material, the i_{corr} value is 0.54 µA/cm² and it is decreased after the brazing test to 0.17 µA/cm². In a similar trend, the polarization resistance Rp is also much lower, at 6.137 Ω/cm², after the braze test when compared to the cold-rolled state (17.295 Ω/cm²). Finally, the corrosion rate V_{corr} value, expressed in the µm/year, is lower for material after the braze test compared to the same material before it in the cold-rolled condition.
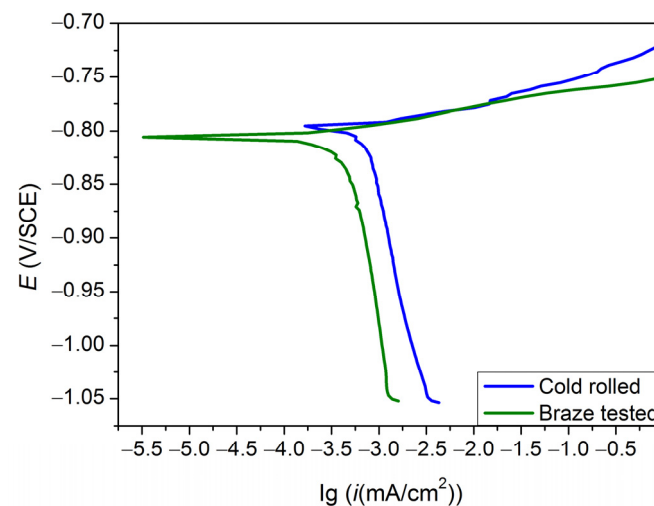

Figure 6. Corrosion results of SWAAT for 0.3 mm cladded material after cold rolling (blue) and after 600 °C—3 min braze test (green).

Table 4. Corrosion parameters calculated from Tafel region.

Sample	E_{corr} (mV)	E_{pit} (mV)	E_{rep} (mV)	$E_{corr}-E_{rep}$ (mV)	i_{corr} (µA/cm²)	R_{p} (Ω/cm²)	V_{corr} (µm/Year)
Cold-rolled	−796	−670	−685	0.125	0.54	17.295	5.91
Braze test	−806	−630	−680	0.126	0.17	6.137	1.81

3.6. Recycling Possibility

In Table 5, the chemical compositions of remelted cladded alloys are presented. Observing the predominant elements Mn and Si, the content of the first one remains stable and unchanged after all three repetitions of remelting. Unlike the Si content, which gradually decreases after the third remelting, there is also a loss of 0.02 wt.% for Fe and 0.01 wt.% for Mg after the second remelting. The content of Cu and Ti remains the same as Mn, unchanged after all three remeltings of cladded material. In accordance with the analyzed chemical compositions, the cooling curves after each remelting (Figure 7) represent similar characteristics with small deviations. The green cooling curve belongs to the sample after the first remelting and has the liquid temperature (T_L) at 663 °C and the temperature of solidification (T_S) at 569 °C. According to the minor deviations in the chemical composition,

the blue cooling curve (sample after the second remelting) and red cooling curve (sample after the third remelting) have T_L at 662 °C or 661 °C and T_S at 571 °C or 566 °C. The highest difference between T_S values is 5 °C.

Table 5. Chemical composition of re-melted cladded Al alloy (wt.%).

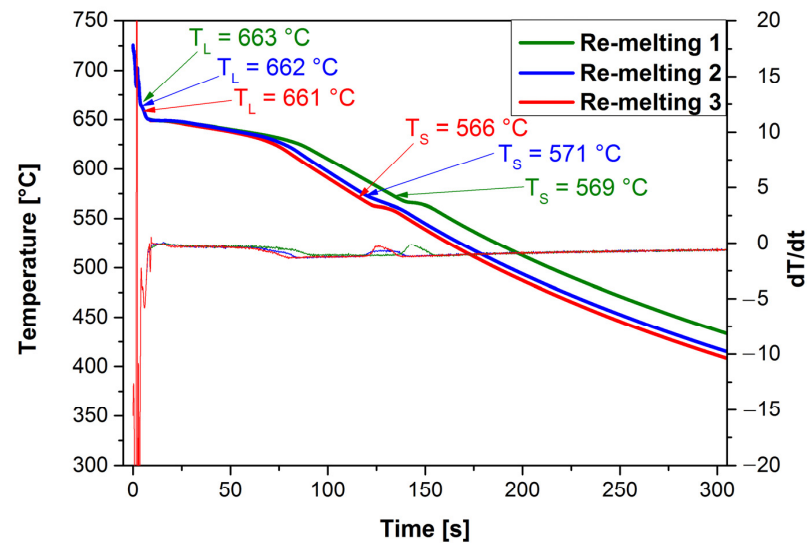| Sample	Mn	Si	Fe	Mg	Cu	Ti	Al
Re-melting 1	0.99	1.56	0.48	0.02	0.07	0.02	Bal.
Re-melting 2	0.99	1.56	0.46	0.01	0.07	0.02	Bal.
Re-melting 3	0.99	1.49	0.46	0.01	0.07	0.02	Bal.

Figure 7. Cooling curves after first re-melting (green), second re-melting (blue), and third re-melting (red).

According to the analyzed chemical compositions, the EN AW 3003 material cladded with EN AW 4343 can be recycled and reused for EN AW 4007 alloy. The chemical composition of the mentioned aluminum alloy fits within the borders of standard composition without any additions. EN AW 4007 is common in rolling and extrusion processes, with its major application field being in welding and soldering. Furthermore, there are possibilities for EN AW 4115 and EN AW 4017 production from cladded material. With the addition of Mg to the recycled material, the chemical compositions will match the alloys commonly used for prepainted aluminum composite panels (PVDF) and treaded sheet as rolled thicker semi-products. The combination of Mg and Cu addition to the chemical composition of remelted clad material will produce the alloy according to the standard composition for EN AW 4025. The promising prospect also includes the addition of Zn, which enables the creation of EN AW 4016 from the remelted cladded rolled products. EN AW 4016 is commonly used for different extruded profiles found in civil engineering applications. Not only in aluminum alloys from the 4xxx series, but the pre-consumer or post-consumer cladded material can also be recycled for the production of EN AW 5025, where Mg, Cu, and Zr must be added to match the standard chemical composition. The mentioned alloy from the 5xxx series is produced as thicker rolled semi-products as well as extruded profiles and tubes needed in civil and mechanical engineering applications. The recycling of EN AW 3003 cladded with EN AW 4343 can also be an option for reproducing the two standard aluminum alloys from the 6xxx series. EN AW 6012 and its variation A (EN AW 6012A) are used for extruded rods, bars, and tubes [25,26]. Additionally, Mg must be added to the analyzed chemical composition to successfully create EN AW 6012 found also in rolled thicker products between 4 mm and 6 mm. The widely used EN AW 6026 in the automotive industry is the next possible solution for the recycling of cladded aluminum alloy. With

the addition of Mg and Cu, the alloy can be used for hot forging, decorative anodizing, hard anodizing of electrical and electronic parts, and especially high-speed automatic lathe applications [27,28]. Besides the production of wrought aluminum alloys from cladded material, there are more possibilities to create casting used aluminum alloys, where the presence of higher content of Si is not an obstacle [29–31].

4. Conclusions

The preparation of EN AW 3003 material cladded with the EN AW 4343 alloy via roll bonding is proposed in this paper. The research is carried out by adopting a combination of numerical simulations, industrial cold rolling, and extensive characterization methods. The conclusions are as follows:

- The rolling force from industrial measurements fits more with the numerically simulated predictions of cladded 3003 material, despite the measured surface temperature being more correlated with the uncladded 3003 material used in the numerical simulation. The most rational explanation of cold rolling parameters for material cladded on both sides was made as a combination of cladded and uncladded material predictions.
- The crystal grains in the cladded layers are significantly bigger than in the core, which gives the impression that the grains in the cladded layers were melted and retake the shape of dendrites. The border between the core and cladded layers is less significant after the braze test compared to the cold-rolled condition, since the grains (dendrites) according to Ostwald ripening interfered with the core layer.
- Corrosion potential, current density, re-passivation potential, and polarization resistance values are lower for heat-treated material at the same thickness compared to the cold-rolled state. In accordance, the corrosion velocity is also lower for material after the braze test (1.81 μm/year), whereas the same material before it in the cold-rolled condition reached 5.91 μm/year.
- The content of Mn is stable and unchanged after all three repetitions of remelting, unlike the Si content, which gradually decreases after the third remelting. According to the analyzed chemical compositions, the cladded material can be recycled and reused as different 4xxx, 5xxx, and 6xxx alloys.

Author Contributions: Conceptualization, B.K.; Methodology, P.C.; Software, M.A.; Investigation, J.K.; Data curation, M.A.; Writing—original draft, J.K.; Writing—review and editing, P.C. and M.A.; Visualization, B.K. All authors have read and agreed to the published version of the manuscript.

Data Availability Statement: The data presented in this study are available on request from the corresponding author. The data are not publicly available due to privacy.

Conflicts of Interest: The authors declare no conflicts of interest.

References

1. Rizvi, S.W.H.; Agrawal, S.; Murtaza, Q. Automotive Industry and Industry 4.0-Circular Economy Nexus through the Consumers' and Manufacturers' Perspectives: A Case Study. *Renew. Sustain. Energy Rev.* **2023**, *183*, 113517. [CrossRef]
2. Zhao, Y.Y.; Zhang, Z.Y.; Jin, L.; Dong, J. Effects of Annealing Process on Sagging Resistance of Cold-Rolled Three-Layer Al Alloy Clad Sheets. *Trans. Nonferrous Met. Soc. China (Engl. Ed.)* **2016**, *26*, 2542–2551. [CrossRef]
3. Miller, W.S.; Zhuang, L.; Bottema, J.; Wittebrood, A.J.; De Smet, P.; Haszler, A.; Vieregge, A. *Recent Development in Aluminium Alloys for the Automotive Industry*; Elsevier: Amsterdam, The Netherlands, 2000; Volume 280.
4. Rezaii, A.; Shafiei, E.; Ostovan, F.; Daneshmanesh, H. Experimental & Theoretical Investigation of Roll Bonding Process of Multilayer Strips by Finite Element Method. *J. Manuf. Process.* **2020**, *54*, 54–69. [CrossRef]
5. Khan, H.A.; Asim, K.; Akram, F.; Hameed, A.; Khan, A.; Mansoor, B. Roll Bonding Processes: State-of-the-Art and Future Perspectives. *Metals* **2021**, *11*, 1344. [CrossRef]
6. Mikhaylovskaya, A.V.; Mochugovskiy, A.G.; Kotov, A.D.; Yakovtseva, O.A.; Gorshenkov, M.V.; Portnoy, V.K. Superplasticity of Clad Aluminium Alloy. *J. Mater. Process. Technol.* **2017**, *243*, 355–364. [CrossRef]
7. Shin, J.; Kim, K.; Ko, S. Effects of Ti Addition into Core Alloy on Forming and Brazing Characteristics of 4343/3003/4343 Aluminum Alloy Clad Sheets. *Mater. Trans.* **2013**, *54*, 2131–2138. [CrossRef]

8. Kang, M.; Zhou, L.; Deng, Y.; Luo, Y.; He, M.; Zhang, N.; Huang, Z.; Dong, L. Microstructure and Mechanical Properties of 4343/3003/6111/3003 Four-Layer Al Clad Sheets Subjected to Different Conditions. *Metals* **2022**, *12*, 777. [CrossRef]
9. Yoon, J.; Lee, S.; Kim, M. Fabrication and Brazeability of a Three-Layer 4343/3003/4343 Aluminum Clad Sheet by Rolling. *J. Mater. Process. Technol.* **2001**, *111*, 85–89. [CrossRef]
10. Kim, S.H.; Kim, H.W.; Euh, K.; Kang, J.H.; Cho, J.H. Effect of Wire Brushing on Warm Roll Bonding of 6XXX/5XXX/6XXX Aluminum Alloy Clad Sheets. *Mater. Des.* **2012**, *35*, 290–295. [CrossRef]
11. Zhang, X.P.; Yang, T.H.; Castagne, S.; Wang, J.T. Microstructure; Bonding Strength and Thickness Ratio of Al/Mg/Al Alloy Laminated Composites Prepared by Hot Rolling. *Mater. Sci. Eng. A* **2011**, *528*, 1954–1960. [CrossRef]
12. Zhang, X.P.; Yang, T.H.; Castagne, S.; Gu, C.F.; Wang, J.T. Proposal of Bond Criterion for Hot Roll Bonding and Its Application. *Mater. Des.* **2011**, *32*, 2239–2245. [CrossRef]
13. Movahedi, M.; Kokabi, A.H.; Madaah-Hosseini, H.R.; Kiani, M. Roll Bonding Behaviour of Al-3003/Al-4043 and Al-3003/Zn Sheets. *Met. Mater. Int.* **2011**, *17*, 665–670. [CrossRef]
14. Kim, S.H.; Kang, J.H.; Euh, K.; Kim, H.W. Grain-Structure Evolution of Brazing-Treated A4343/A3003/A4343 Aluminum Brazing Sheets Rolled with Different Reductions. *Met. Mater. Int.* **2015**, *21*, 276–285. [CrossRef]
15. Cha, J.H.; Kim, S.H.; Lee, Y.S.; Kim, H.W.; Choi, Y.S. Effect of Heat Treatment on Interfacial and Mechanical Properties of A6022/A7075/A6022 Roll-Bonded Multi-Layer Al Alloy Sheets. *Met. Mater. Int.* **2016**, *22*, 880–886. [CrossRef]
16. Raabe, D.; Ponge, D.; Uggowitzer, P.J.; Roscher, M.; Paolantonio, M.; Liu, C.; Antrekowitsch, H.; Kozeschnik, E.; Seidmann, D.; Gault, B.; et al. Making Sustainable Aluminum by Recycling Scrap: The Science of "Dirty" Alloys. *Prog. Mater. Sci.* **2022**, *128*, 100947. [CrossRef]
17. Pilipenets, O.; Gunawardena, T.; Kin Peng Hui, F.; Nguyen, K.; Mendis, P.; Aye, L. Upcycling Opportunities and Potential Markets for Aluminium Composite Panels with Polyethylene Core (ACP-PE) Cladding Materials in Australia: A Review. *Constr. Build. Mater.* **2022**, *357*, 129194. [CrossRef]
18. Chen, X.; Zhang, B.; Du, Y.; Liu, M.; Bai, R.; Si, Y.; Liu, B.; Jung, D.W.; Osaka, A. Constitutive Model Parameter Identification Based on Optimization Method and Formability Analysis for Ti6Al4V Alloy. *Materials* **2022**, *15*, 1748. [CrossRef] [PubMed]
19. Li, Z.; Rezaei, S.; Wang, T.; Han, J.; Shu, X.; Pater, Z.; Huang, Q. Recent Advances and Trends in Roll Bonding Process and Bonding Model: A Review. *Chin. J. Aeronaut.* **2023**, *36*, 36–74. [CrossRef]
20. Prakash, A.; Nöhring, W.G.; Lebensohn, R.A.; Höppel, H.W.; Bitzek, E. A Multiscale Simulation Framework of the Accumulative Roll Bonding Process Accounting for Texture Evolution. *Mater. Sci. Eng. A* **2015**, *631*, 104–119. [CrossRef]
21. Wang, H.; Su, L.; Yu, H.; Lu, C.; Kiet Tieu, A.; Liu, Y.; Zhang, J. A New Finite Element Model for Multi-Cycle Accumulative Roll-Bonding process and experiment verification. *Mater. Sci. Eng. A* **2018**, *726*, 93–101. [CrossRef]
22. Kim, J.K.; Huh, M.Y.; Jee, K.K.; Engler, O. Texture Evolution during Roll-Cladding of a Composite of Five Plies of Ferritic Stainless Steel and Aluminum Sheets. In *Materials Science Forum*; Trans Tech Publications Ltd.: Bäch, Switzerland, 2005; Volume 495–497, pp. 1681–1686.
23. Bernardi, C.; Hazotte, A.; Siredey-Schwaller, N.; Mazet, T.; Lacaze, J.; Mi, J.L. Microstructure Evolution in an Aluminum Cladded Sheet during Vacuum Brazing. In *Materials Science Forum*; Trans Tech Publications Ltd.: Bäch, Switzerland, 2014; Volume 790, pp. 355–360. [CrossRef]
24. Shahani, A.J.; Xiao, X.; Skinner, K.; Peters, M.; Voorhees, P.W. Ostwald Ripening of Faceted Si Particles in an Al-Si-Cu Melt. *Mater. Sci. Eng. A* **2016**, *673*, 307–320. [CrossRef]
25. Viceré, A.; Roventi, G.; Paoletti, C.; Cabibbo, M.; Bellezze, T. Corrosion Behavior of Aa6012 Aluminum Alloy Processed by Ecap and Cryogenic Treatment. *Metals* **2019**, *9*, 408. [CrossRef]
26. Yao, E.; Zhang, H.; Ma, K.; Ai, C.; Gao, Q.; Lin, X. Effect of deep cryogenic treatment on microstructures and performances of aluminum alloys: A review. *J. Mater. Res. Technol.* **2023**, *26*, 3661–3675. [CrossRef]
27. Jovičević-Klug, M.; Rezar, R.; Jovičević-Klug, P.; Podgornik, B. Influence of Deep Cryogenic Treatment on Natural and Artificial Aging of Al-Mg-Si Alloy EN AW 6026. *J. Alloys Compd.* **2022**, *899*, 163323. [CrossRef]
28. Abas, M.; Sayd, L.; Akhtar, R.; Khalid, Q.S.; Khan, A.M.; Pruncu, C.I. Optimization of machining parameters of aluminum alloy 6026-T9 under MQL-assisted turning process. *J. Mater. Res. Technol.* **2020**, *5*, 10916–10940. [CrossRef]
29. Li, Y.; Hu, A.; Fu, Y.; Liu, S.; Shen, W.; Hu, H.; Nie, X. Al Alloys and Casting Processes for Induction Motor Applications in Battery-Powered Electric Vehicles: A Review. *Metals* **2022**, *12*, 216. [CrossRef]
30. Jo, Y.H.; Moon, H.-R.; Bae, J.W.; Yoo, J.; Lee, S.G.; Lee, Y.-S.; Kim, H.-W. Effects of casting speed on microstructural and tensile properties of AleMgeSi alloy fabricated by horizontal and vertical twin-roll casting. *J. Mater. Res. Technol.* **2023**, *26*, 8010–8024. [CrossRef]
31. Sezunenko, A.Y.; Petryshyn, M.M.; Kolesnichenko, A.A.; Lytvyn, R.V.; Lukianenko, I.V.; Byba, I.G.; Yamshinskij, M.M.; Barabash, M.Y. Features of structure and properties of Al–Si–Cu alloy produced by pressure casting. *Results Mater.* **2024**, *21*, 100539. [CrossRef]